Supplemental Material

Qiang Gao[a], Tingting Lin[b], Wei Wang[a], Guimei Shi[a], Xin Jin[c], Chen Shen[d]

[a]*School of Science, Shenyang University of Technolog, No.111, Shenliao West Road, Shenyang, 110870, China*
[b]*School of Liberal Arts and Sciences, North China Institute of Aerospace Engineering, No. 133, Aimin East Road, Langfang, 065000, China*
[c]*College of Physics and Electronic Engineering, Chongqing Normal University, No. 55, Daxue City South Road, Chongqing, 401331, China*
[d]*Institute of Material Science, TU Darmstadt, Otto-Berndt-Strasse 3, Darmstadt, 64287, Germany*

S1. Structure data

The structure ("POSCAR" file) for the parent monolayer VYN is as following:

```
VYN
   1.00000000000000
     3.2768074094378834    -0.0000000000000000     0.0000000000000000
    -1.6384037047189410     2.8377984598802475    -0.0000000000000000
     0.0000000000000000     0.0000000000000000    25.0000000000000000
   V     Y     N
     1     1     1
Direct
  0.3333333333333357  0.6666666666666643  0.4716678436141983
  0.6666666666666643  0.3333333333333357  0.5622241530749906
  0.0000000000000000  0.0000000000000000  0.5000000000000000
```

The structure ("POSCAR" file) for the functionalized Janus MXene VYN-F_2 is as following:

```
VYNF2
   1.00000000000000
     3.5075436930073574     0.0000000000000000     0.0000000000000000
    -1.7537718465036780     3.0376219430257274     0.0000000000000000
     0.0000000000000000     0.0000000000000000    25.0000000000000000
   V     Y     N     F
     1     1     1     2
Direct
  0.3333333333333357  0.6666666666666643  0.4463458746425601
  0.6666666666666643  0.3333333333333357  0.5471791584750818
  0.0000000000000000  0.0000000000000000  0.5000000000000000
  0.3333333429999996  0.6666666870000029  0.5981807829282459
  0.6666666870000029  0.3333333429999996  0.4092214112224966
```

S2. Structure transformation and spin configurations

As shown in Fig. S1, the primitive cell for both VYN and VYN-F_2 are in the hexagonal lattice. Now we take VYN as an example to show the transformation for the original hexagonal lattice. Based on the hexagonal lattice, the diagonally rectangular lattice is obtained by the perpendicular diagonal lines. The 211-cell is made from the 2×1×1 super cell of the diagonally rectangular lattice.

In both VYN, V is the only magnetic atom. In the 211-cell, there are four V atoms. Based on the 211-cell, one ferromagnetic (FM) and two antiferromagnetic (AFM) spin configurations are considered in the calculations as shown in Fig. S2. In the FM configuration, the exchange coupling for all V atoms are ferromagnetic. In the AFM-1 configuration, the nearest neighbour (NN) interaction is AFM while the next nearest neighbour (NNN) interaction is FM. In the AFM-2 configuration, the NN interaction is FM while the NNN interaction is AFM. It should be noticed the spin configurations are the same for both VYN and VYN-F_2.

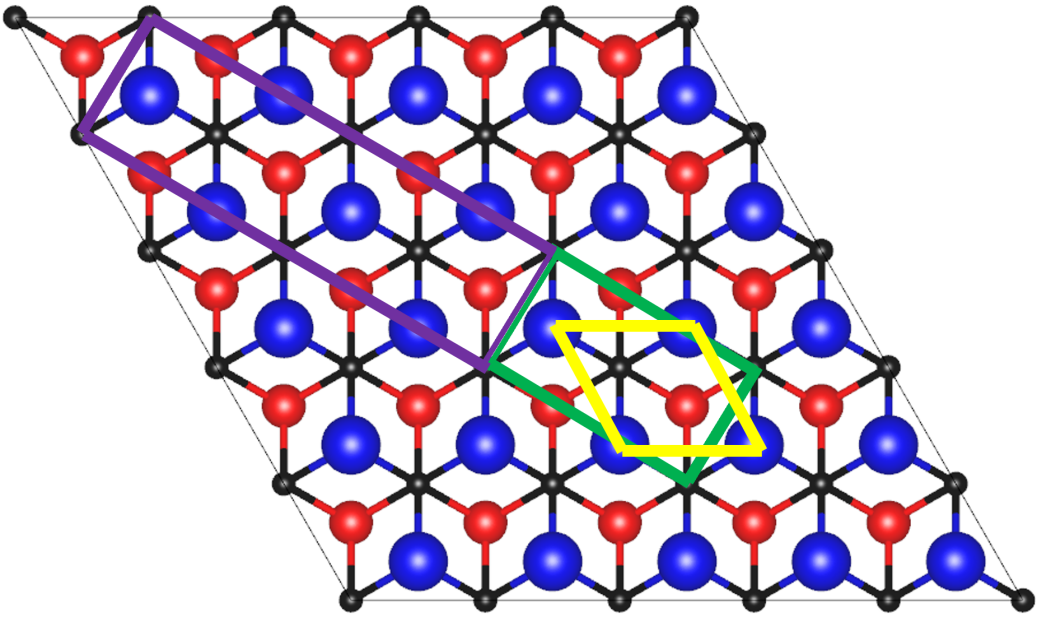

Figure S1: The lattice transformation for VYN. The yellow, green and violet edge lines mark the originally hexagonal, diagonally rectangular, 2×1×1 super cell (for diagonally rectangular) lattices, respectively.

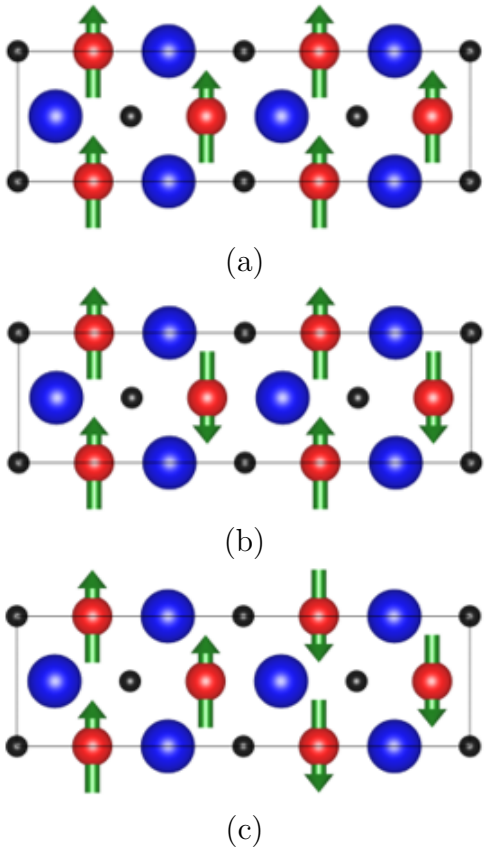

Figure S2: The ferromagnetic (FM) and two anti-ferromagnetic (AFM) spin configurations for VYN. (a) FM, (b) AF-1 and (c) AF-2.

S3. Properties of the parent monolayer VYN

VYN is a metallic ferromagnet as the bands in both spin up and down channels cross Fermi level with a total magnetic moment of 2.15 μ_B, where the V atom makes a leading contribution of 1.72 μ_B to the total magnetic moment (m_V=1.72 μ_B). For VYN, the nearest neighbour (J_{NN}) and next neighbour (J_{NNN})exchange coupling parameters are 3.806 meV and 1.481 meV.

The magnetism of VYN originates from the itinerant electron of V. The condition for a stable itinerant magnetism is the Stoner criterion

$$ID(E_F) > 1, \tag{1}$$

where I is the exchange strength in ferromagnetic order and $D(E_F)$ is the partial density of states (DOS) of V at Fermi level in non-magnetic order for VYN. As is shown in Fig. S3, the partial DOS of V is directly obtained with a value of 4.3067 states/eV ($D(E_F) = 4.3067 states/eV$) at Fermi level. The exchange strength I is associated with the magnetic moment of V atom and average exchange splitting energy $< \Delta\epsilon_k >$. The later parameter is evaluated by the average absolute difference between Kohn-Sham eigenvalues within such spin up and down channels at different k points in the whole Brillouin zone. For V atom in VYN, it is found the average exchange splitting energy $< \Delta\epsilon_k >= 0.489eV$. The exchange strength is calculated through $I = \frac{<\Delta\epsilon_k>}{m_V} = 0.284eV/\mu_B$. Then it is clear that the ferromagnetic order for VYN is stable as the Stoner criterion is satisfied ($ID(E_F) = 1.22 > 1$).

S4. Relative energies of nine phases

There are in total 9 possible phases for the functionalized $VYNF_2$ Janus MXene. The relative energy for each phase is shown in Table S1.

Table S1: The relative energy of each phase with respect to that of the $S_{BB'}$ phase. The energy is in unit of eV/at.

Phase	$S_{AA'}$	$S_{AB'}$	$S_{AC'}$
Energy	0.4550	0.3627	0.5237
Phase	$S_{BA'}$	$S_{BB'}$	$S_{BC'}$
Energy	0.1056	0.0	0.1510
Phase	$S_{CA'}$	$S_{CB'}$	$S_{CC'}$
Energy	0.1376	0.0378	0.1899

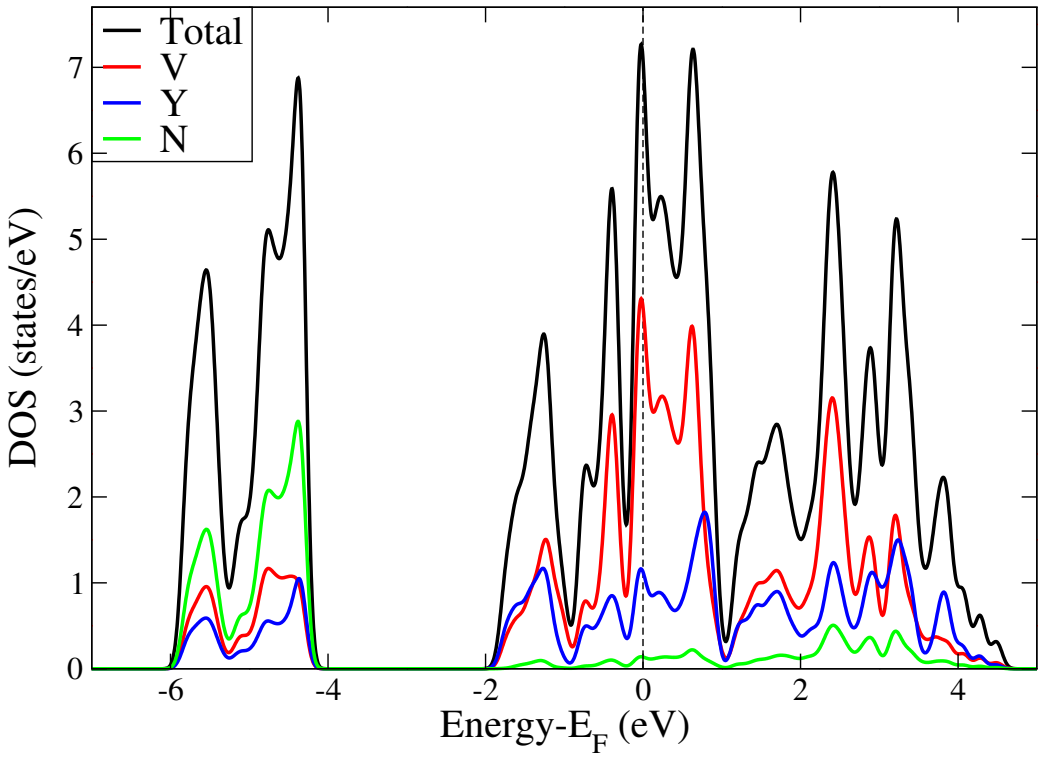

Figure S3: The total density of states (DOS) for Janus MXene VYN together with the corresponding partial DOS (PDOS) for V, Y, and N atoms in non-spinpolarized calculations. The vertical ashed lines denote the Fermi level. The solid black curve is the total DOS for VYN. The red, blue, and green curves represent the partial DOS of V, Y, and N atoms, respectively.

S5. Linear response theory for U_{eff}

The effective potential (U_{eff}) can be evaluated based on linear response theory (LRT) [1]. Applying a series of small potential (α), the number of the occupied electrons (Nocc.) in the considered *d*-orbitals are obtained from density function theory (DFT) calculations by means of both self-consistent (SCF) and non-self-consistent (NSCF). The slopes of SCF (χ_2) and NSCF (χ_1) DFT calculations are by linear fitting the data set of [α, Nocc.]. Accordingly, the effective potential U_{eff} is calculated by

$$U_{eff} = \chi_2^{-1} - \chi_1^{-1}. \tag{2}$$

For the functionalized Janus MXene VYN-F_2, there are two kind of transition atoms. Evaluating U_{eff} for one transition metal element, the on site effective potential for the other transition metal should be turned off. The structure is a newly predicted case. Therefore, the U_{eff} and the lattice should be simultaneously optimized to reach both self consistency [2] as shown in Fig. S4. The LRT process to obtain the effective potential for both V and Y are shown in Fig. S5. After two LRT circle processes, we obtain the final for V and Y as U^V_{eff}=6.09 eV and U^V_{eff}=4.64 eV. Based on such effective potentials, the elastic constants, piezoelectric tensors, the Monte Carlo (MC) simulations, and the strain effect are studied for the functionalized Janus MXene VYN-F_2.

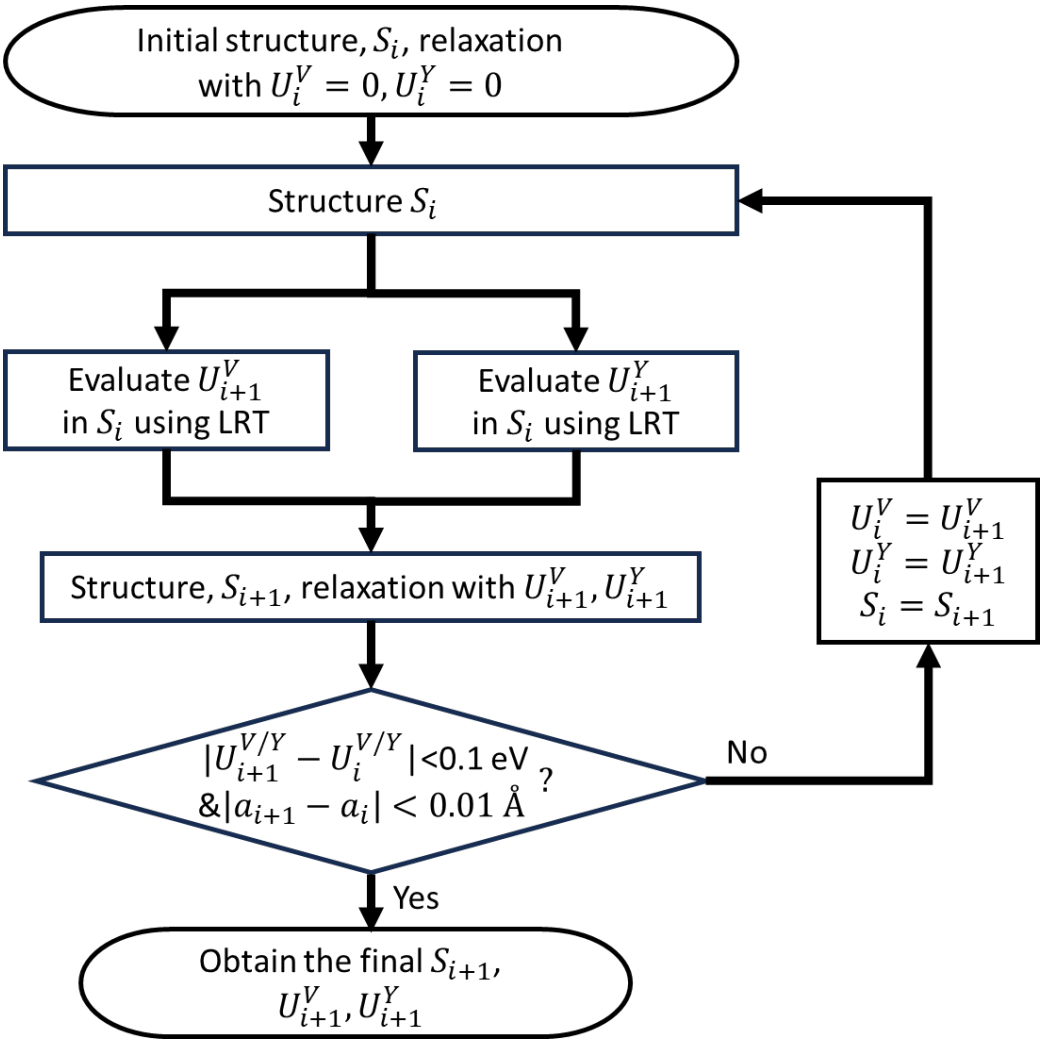

Figure S4: The flow chart to obtain the simultaneously self consistency for both structure and U_{eff} base on the linear response theory (LRT). a_i is the lattice constant for structure S_i.

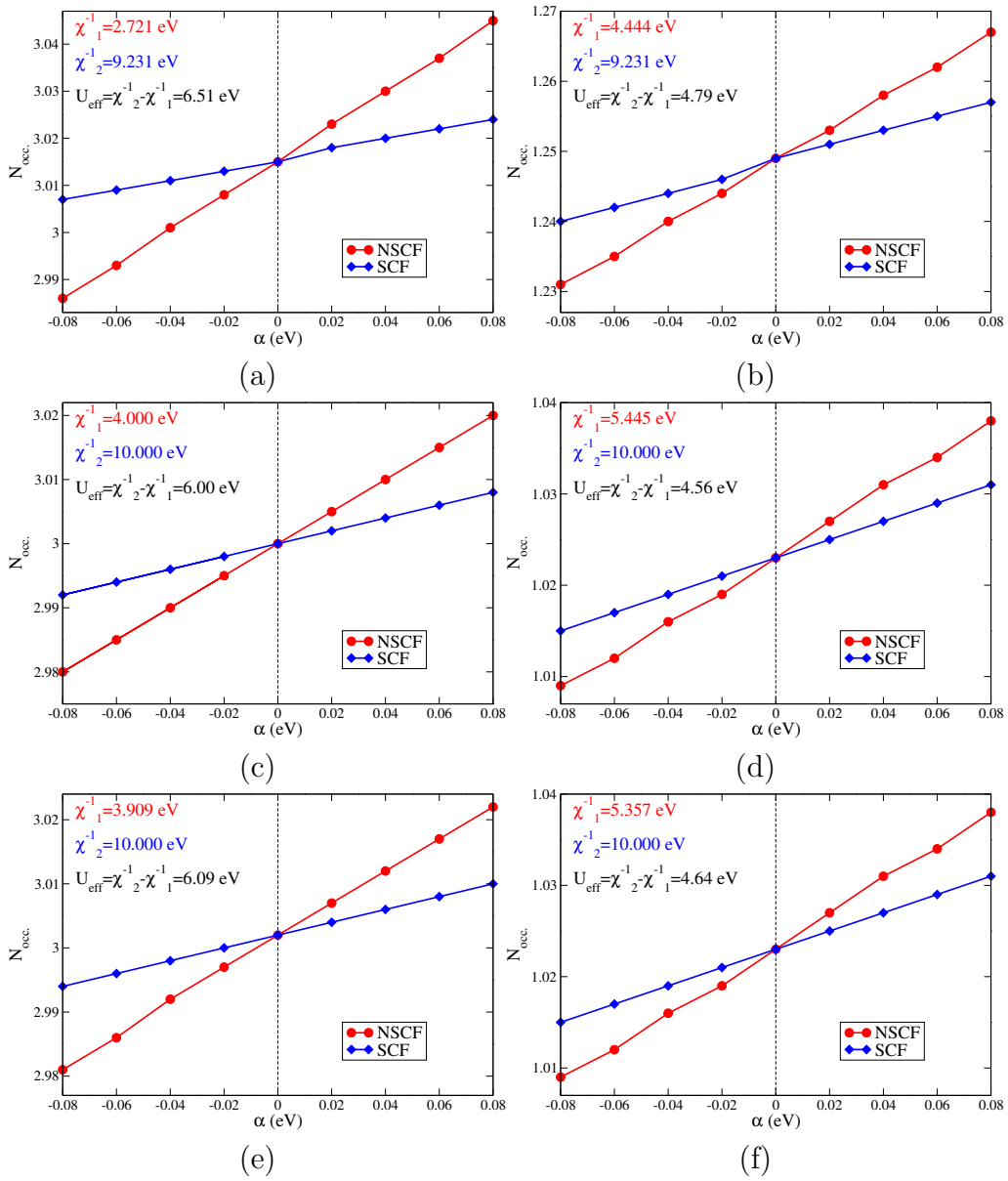

Figure S5: The process to obtain the effective potential for V and Y atoms based on linear response theory (LRT). (a), (c), (e) are the linear response theory (LRT) results for V, while (b), (d), (f) are the LRT results for Y. (a) and (b) is calculated based on the initial structure (U_i^Y=0 and U_i^V=0). (c) and (d) is the first circle process in Fig. S4, while (e) and (f) are the second circle in Fig. S4. In each sub-figure, the red circle and blue square data denote number ($N_{occ.}$) of occupied d electrons for V (or Y) as a function of the small potential (α). The dashed line is the point with no potential.

S6. Strain effects

Under a strain in the range of $-5\% \leq x \leq 5\%$, the exchange coupling parameters of the nearest neighbour (J_{NN}) and next nearest neighbour (J_{NNN}) interactions are shown in Fig. S13. Hereafter, the Néel temperature (T_N) for the functionalized Janus MXene VYN-F_2 are evaluated by means of Monte Carlo algorithm based on Ising model as implanted in the VAMPIRE code [3], using a 100×100 2D super cell to avoid boundary effect with 300 000 steps at each temperature to reach thermal equilibrium. Substituting the exchange coupling parameters, the Monte Carlo simulations for VYN-F_2 under strain in the compressive ($-5\% \leq x \leq 0\%$) and tensile ($0\% \leq x \leq 5\%$) strain range are shown in Figs. S7 and S8, respectively. The "UCF" file includes the exchange coupling parameters, the basis of the lattice, and lattice constants, which is a main input file for Monte Carlo simulations in VAMPIRE code. One typical "UCF" file for the functionalized Janus MXene VYN-F_2 under no strain is as following:

```
# Unit cell size:
3.5075436930073574 3.5075436930073574 25.0
# Unit cell vectors:
1.0 0.0 0.0
0.5 0.8660254038 0.0
0.0 0.0 1.0
# Atoms num, id cx cy cz #  mat lc hc not important
1
0 0.1 0.1 0.0 0 1 2
# Interactions n exctype, id i j dx dy dz Jij
12 isotropic
0     0 0    1    0    0     -1.680227e-22
1     0 0    0    1    0      1.680227e-22
2     0 0   -1    0    0     -1.680227e-22
3     0 0    0   -1    0      1.680227e-22
4     0 0    1   -1    0     -1.680227e-22
5     0 0   -1    1    0     -1.680227e-22
6     0 0    1    1    0     -8.3154e-24
7     0 0   -1   -1    0     -8.3154e-24
8     0 0    1   -2    0     -8.3154e-24
9     0 0   -1    2    0     -8.3154e-24
10    0 0    2   -1    0      8.3154e-24
11    0 0   -2    1    0     8.3154e-24
```

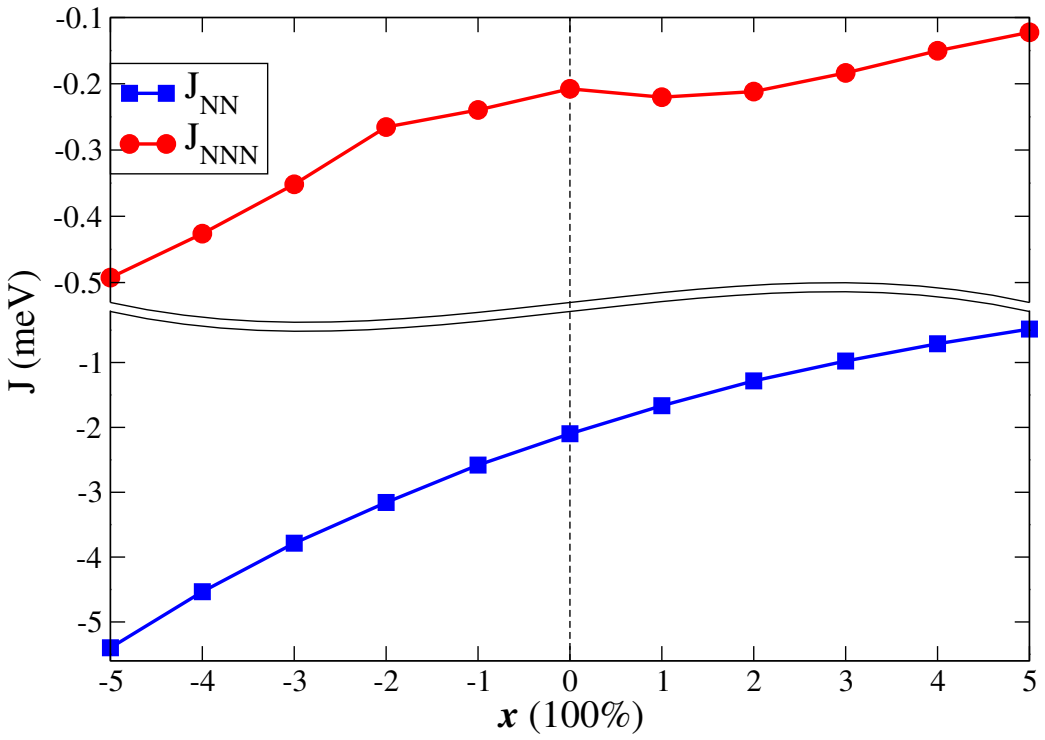

Figure S6: The exchange parameters for the nearest neighbour (J_{NN}) and next nearest neighbour (J_{NNN}) coupling interactions under strain in the range of $-5\% \leq x \leq 5\%$. The dashed line denote the compound is under no strain.

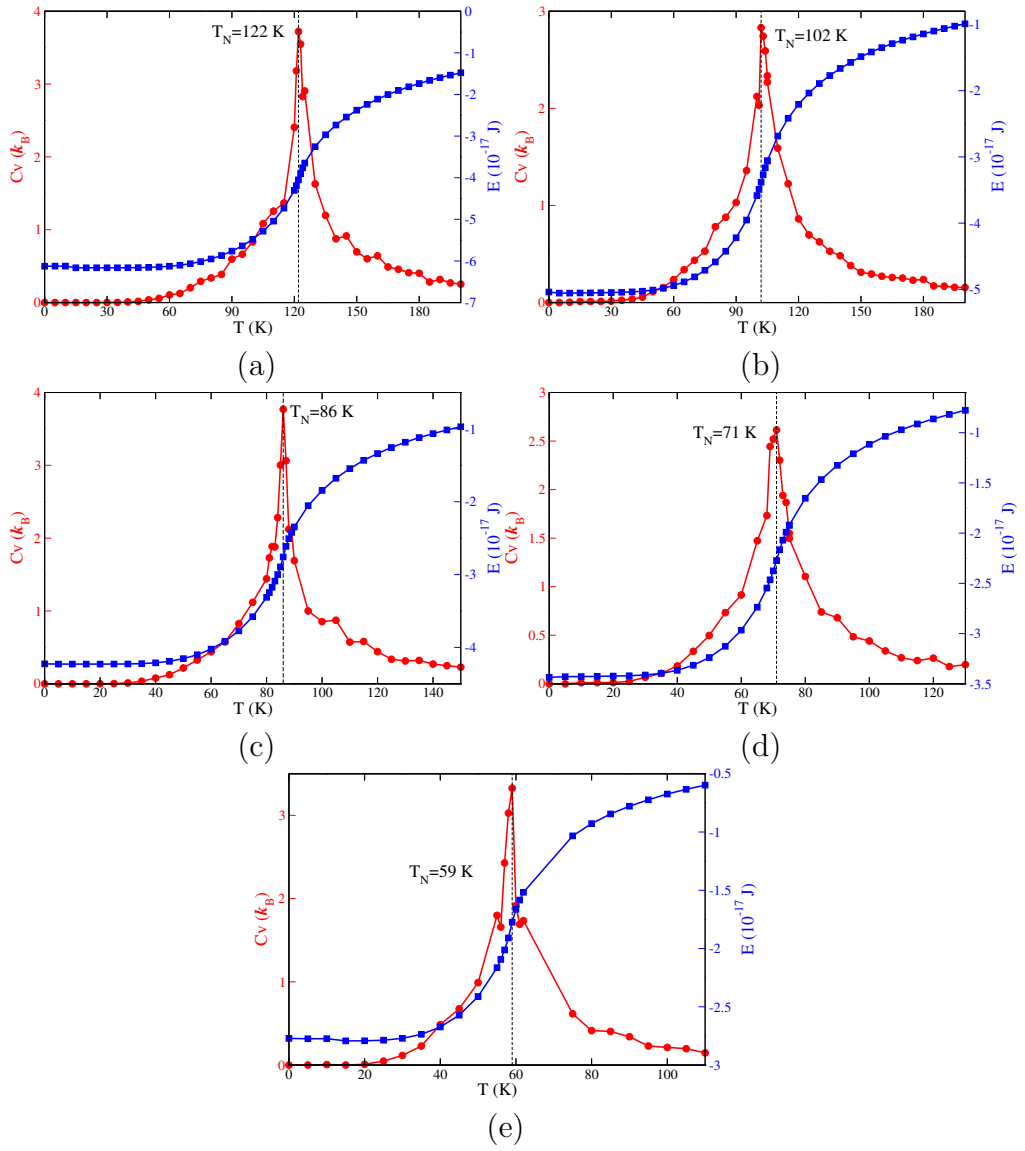

Figure S7: The Monte Carlo simulation results for the functionalized Janus MXene VYN-F_2 under compressive strain. (a), (b), (c), (d), and (e) represents respectively the Monte Carlo simulation results with the strain of x =-5%, -4%, -3%, -2%, and -1%. The dashed line denote the Néel temperature point. In each sub-figure, the red circle and blue square data mark the specific heat (C_V) and internal energy (E) as a function of temperature (T).

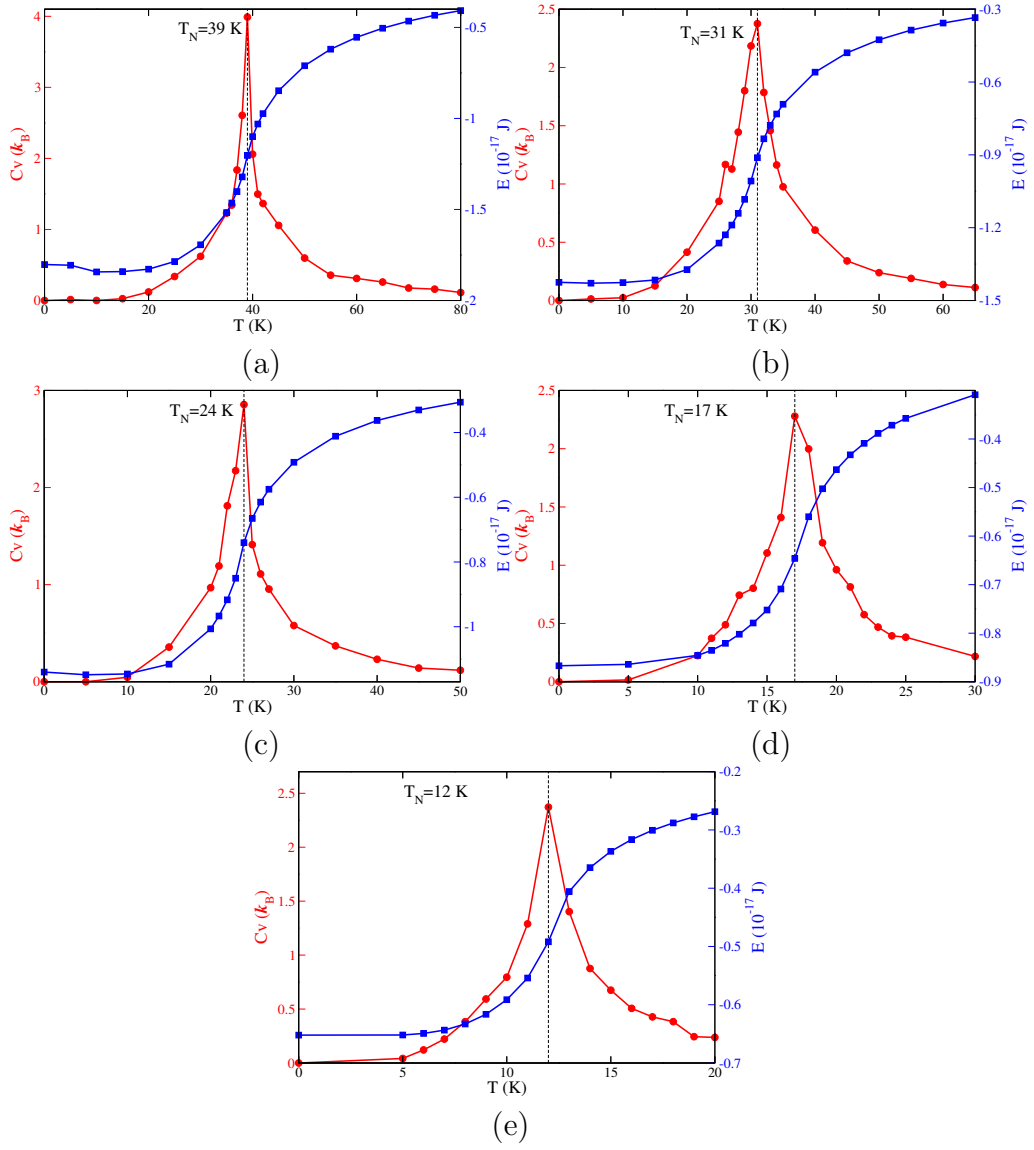

Figure S8: The Monte Carlo simulation results for the functionalized Janus MXene VYN-F_2 under tensile strain. (a), (b), (c), (d), and (e) represents respectively the Monte Carlo simulation results with the strain of x =1%, 2%, 3%, 4%, and 5%. The dashed line denote the Néel temperature point. In each sub-figure, the red circle and blue square data mark the specific heat (C_V) and internal energy (E) as a function of temperature (T).

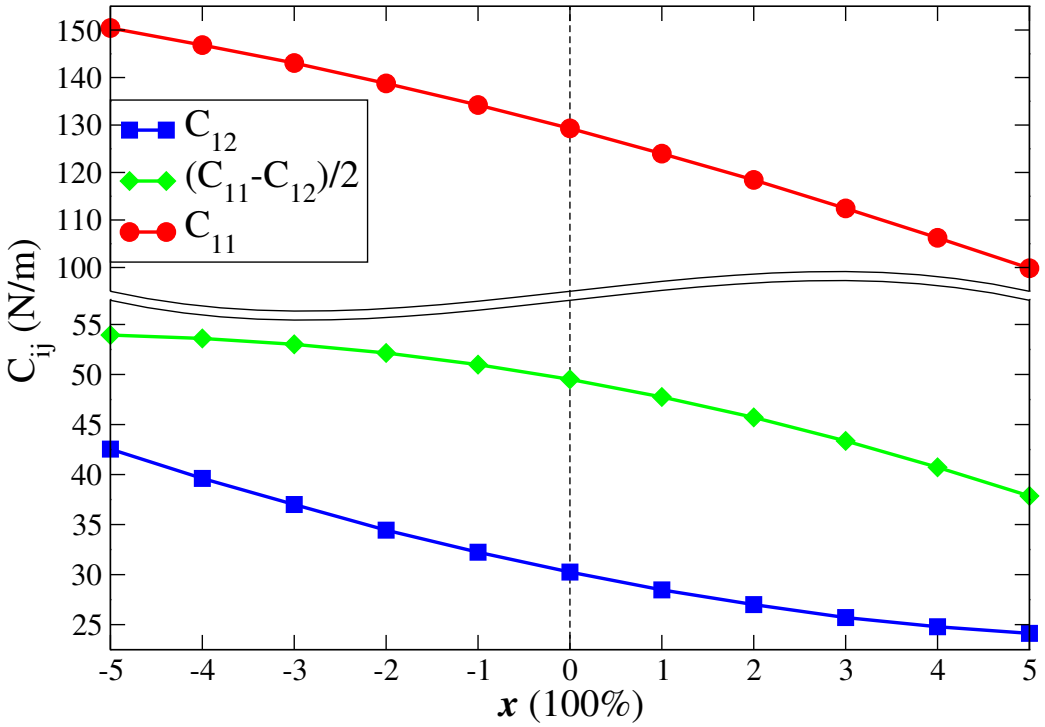

Figure S9: The elastic constants as a function of strain for the functionalized Janus MXene VYN-F_2 in the range of $-5\% \leq x \leq 5\%$. The blue square, red circle, and green diamond data denote the C_{12}, C_{11}, and C_{33} components of the elastic constants, respectively. The dashed line means the compound is under no strain.

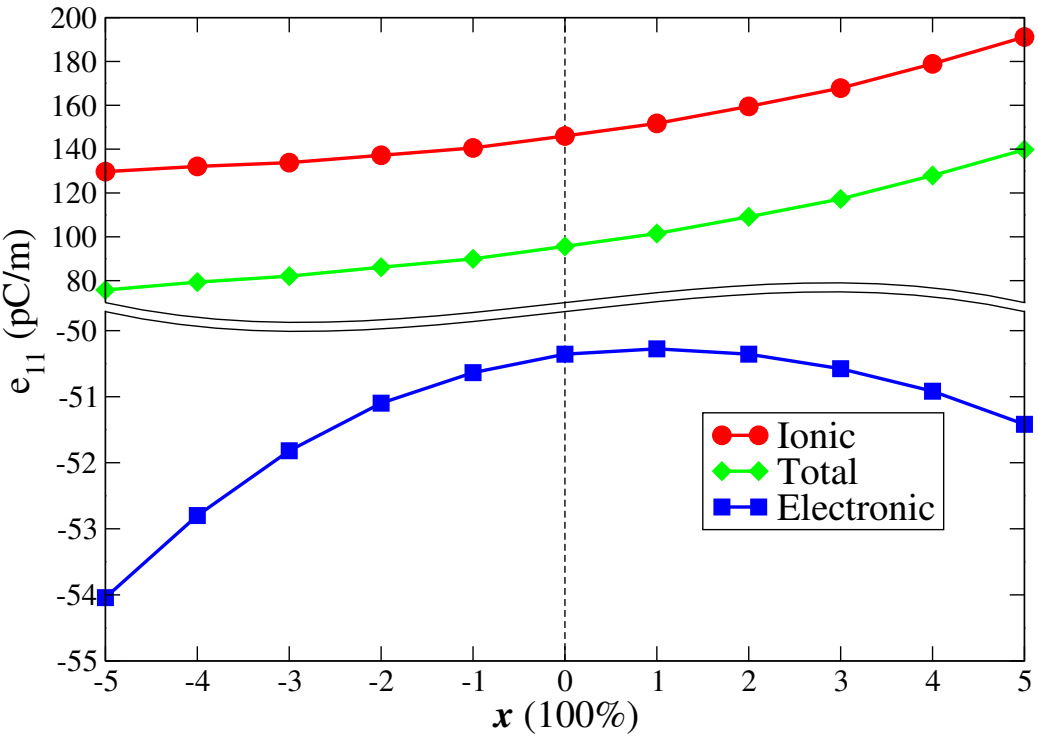

Figure S10: The in-plane piezoelectric stress tensor (e_{11}) as a function of strain for the functionalized Janus MXene VYN-F_2 in the range of $-5\% \leq x \leq 5\%$. The blue square, red circle, and green diamond data denote the electronic contribution, ionic contribution, and total value of e_{11}, respectively. The dashed line means the compound is under no strain.

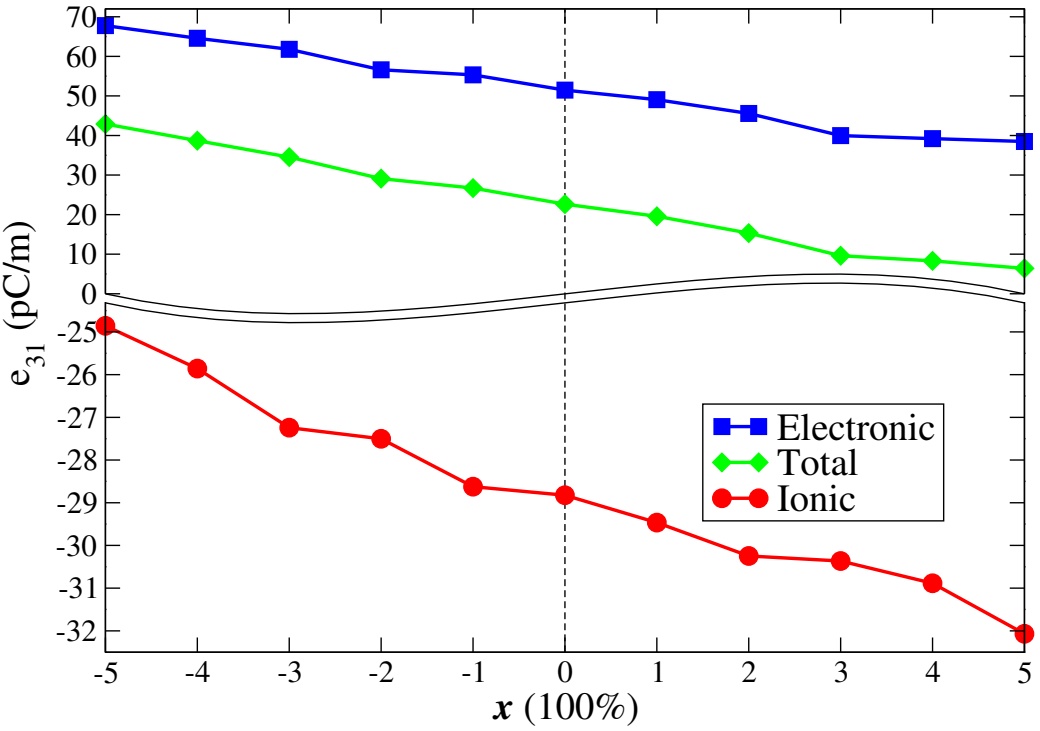

Figure S11: The out-off-plane piezoelectric stress tensor (e_{31}) as a function of strain for the functionalized Janus MXene VYN-F_2 in the range of $-5\% \leq x \leq 5\%$. The blue square, red circle, and green diamond data denote the electronic contribution, ionic contribution, and total value of e_{31}, respectively. The dashed line means the compound is under no strain.

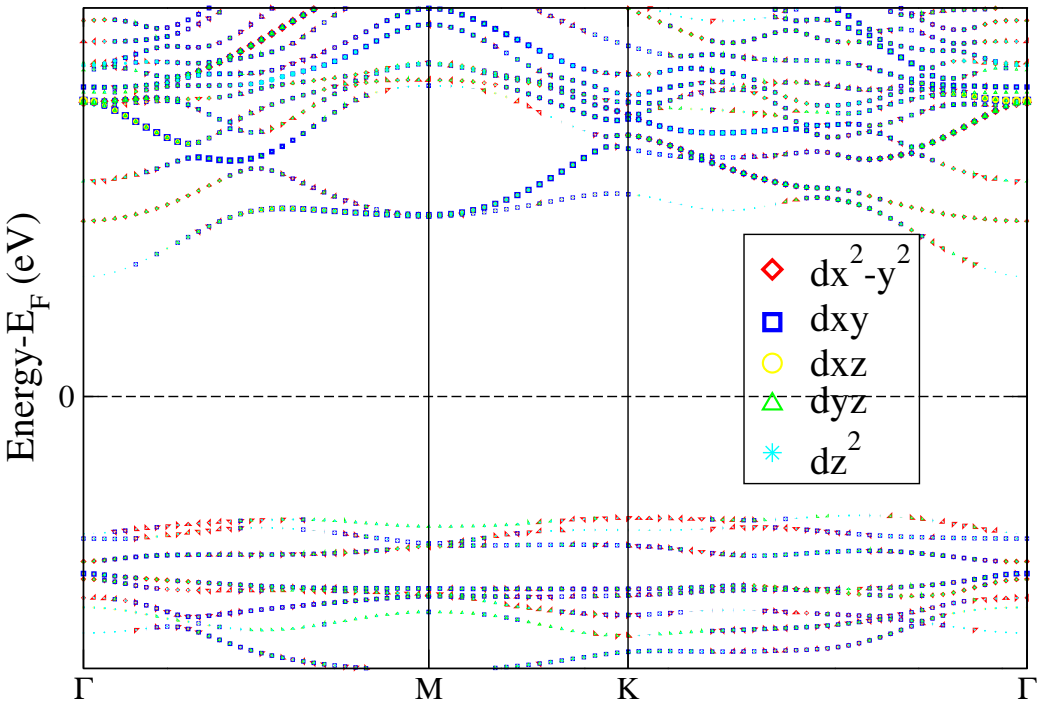

Figure S12: The projected band structures of *d*-orbital of Y atom in $VYNF_2$.

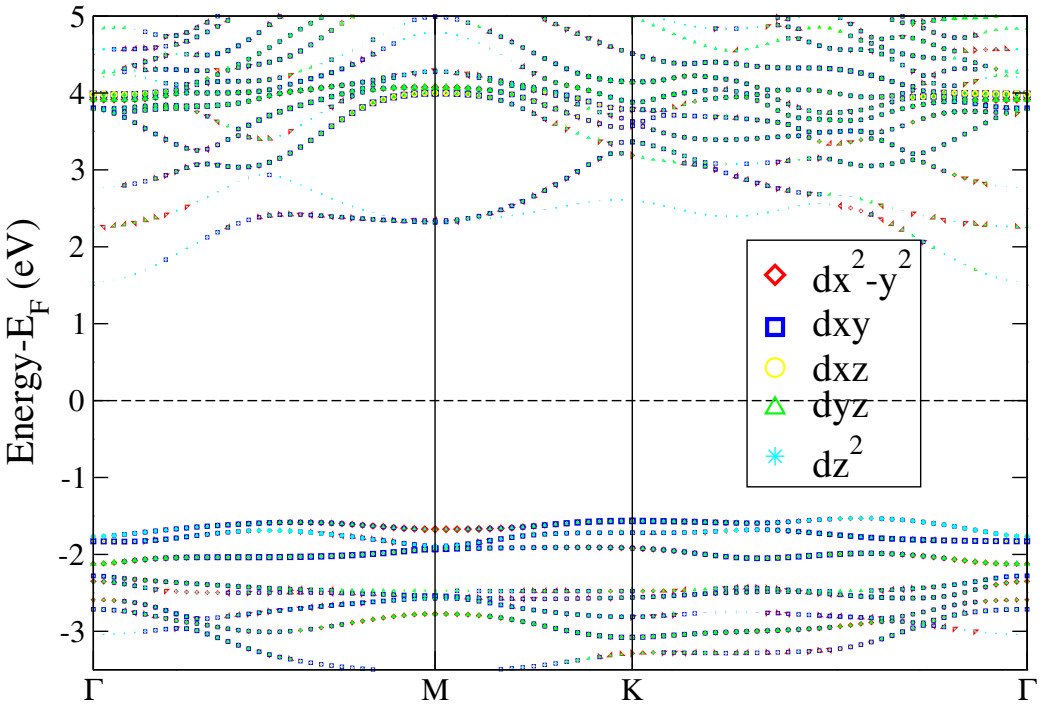

Figure S13: The projected band structures of *d*-orbital of V atom in $VYNF_2$.

References

[1] M. Cococcioni and S. De Gironcoli, *Physical Review B—Condensed Matter and Materials Physics*, 2005, **71**, 035105

[2] G. Lan, J. Song and Z. Yang, *Journal of Alloys and Compounds*, 2018, **749**, 909–925

[3] R. F. Evans, W. J. Fan, P. Chureemart, T. A. Ostler, M. O. Ellis and R. W. Chantrell, *Journal of Physics: Condensed Matter*, 2014, **26**, 103202